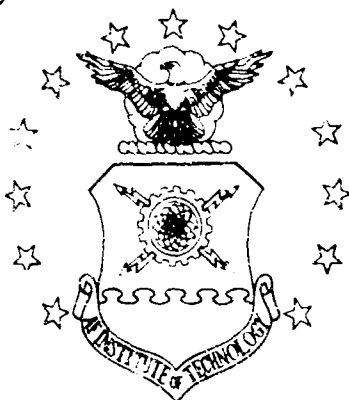
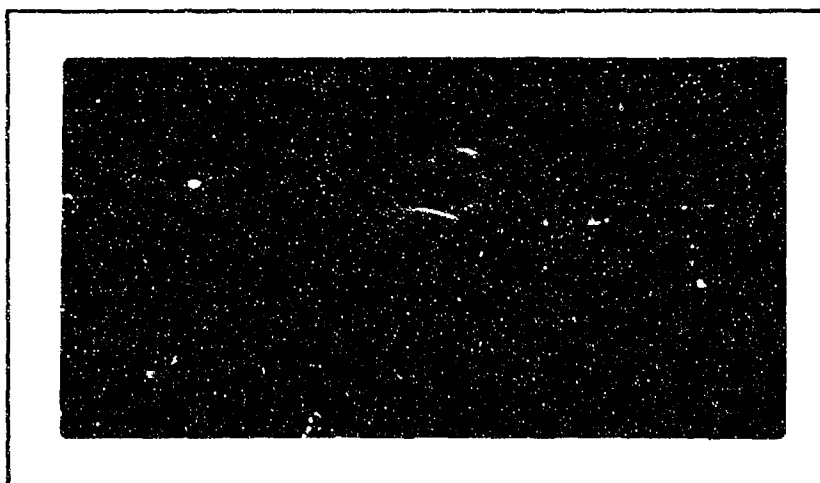


AD 672973

AIR FORCE INSTITUTE OF TECHNOLOGY



AIR UNIVERSITY
UNITED STATES AIR FORCE



SCHOOL OF ENGINEERING

WRIGHT-PATTERSON AIR FORCE BASE, OHIO

Reproduced by the
CLEARINGHOUSE
for Center of Scientific & Technical
Information, Springfield, Va. 22151

AUG 15 1968

BALLISTIC IMPACT FLASH

THESIS

GAW/MC/68-1

John Billy Abernathy
Captain USAF

This document has been approved for
public release and sale; its distri-
bution is unlimited.

BALLISTIC IMPACT FLASH

THESIS

Presented to the Faculty of the School of Engineering of
the Air Force Institute of Technology

Air University

in Partial Fulfillment of the
Requirements for the Degree of

Master of Science

By

John Billy Abernathy
Captain USAF

Graduate Air Weapons

June 1968

This document has been approved for
public release and sale; its distri-
bution is unlimited.

Preface

This report is the result of my attempt to expand the knowledge available in the area of ballistic impact flash. My principle concern has been the temperature of the down range flash caused by fragment simulators on aluminum plates.

The author is indebted to many persons who gave valuable assistance in the accomplishment of this study. I wish to thank Mr. Lillard E. Gilbert of the Air Force Flight Dynamics Laboratory for making the gun range and crew available; Mr. V. L. Mangold for equipment; Mr. G. E. Maddux for photographic help; Mr. B. B. Neal for the use of the spectrograph; Dr. L. C. Long for helpful guidance; the faculty members of my thesis committee; Major W. Goldberg, Dr. D. W. Breuer, and Captain J. L. Kurzenberger; and my wife Nancy for being patient.

John B. Abernathy

Contents

	Page
Preface	ii
Table of Contents	iii
List of Figures	v
List of Tables	vi
Abstract	vii
I. Introduction	1
Background	2
II. Physical Model	5
Rupture Phase	5
Ablation Phase	6
Burned Ejecta Phase	6
III. Spectroscopic Temperature Measurement	8
Theory	8
Frequency	9
Population	10
Transition Probability	11
IV. Experimental Method	14
V. Results	20
VI. Discussion of Results and Conclusions	27
VII. Recommendations	33
Bibliography	34
Appendix A: Description of Equipment	37
1. Flight Dynamics Laboratory Fragment Simulator	37

2.	Instrumentation	38
Appendix B:	Film Calibration	44
Appendix C:	Temperature Computation Program	40
Vita		50

List of Figures

Figure	Page
1 Diffusion Film Burning Model	7
2 Potential Energy Levels	12
3 Projectiles	15
4 Image Converter Sequences	16
5 Streak Camera Print	17
6 Spectrographic Alignment	18
7 ALO Green System Spectrum	19
8 Area Ratio	20
9 Time Distance Trace From Least Squares Fit	24
10 Vibrational Temperature	25
11 Photomultiplier Trace	26
12 Target Plate Measurements	28
13 Down Range Flash	29
14 Range Layout	37
15 Streak Camera Image	39
16 TRW 1D Image Converter Camera	40
17 Spectrograph	41
18 Spectrograph Lens System	42

List of Tables

Table	Page
I Image Converter Sequences	16
II Aluminum Projectile Data	22
III Steel Projectile Data	23
IV Down Range Velocity	24
V Relative Intensity for Shot Number A18	26
VI ALO System Excited by Carbon Arc	48
VII ALO System Excited by Aluminum Projectile . .	49

Abstract

The down range flash from the perforation of thin aluminum plates by steel and aluminum fragment simulators; one half inch diameter cylinders with hemispherical heads; was investigated to determine time, size, and temperature. By comparing the relative intensities of vibrational band structure in the AlO green system an effective vibrational temperature for the flash was determined to be between 3400°K and 4100°K . The overall dimensions of the flash were found to be approximately 14 inches long and five inches in diameter. The time duration was found to be between three and five milliseconds.

BALLISTIC IMPACT FLASH

I. Introduction

Once again the United States, engaged in a conventional war, is faced with problems similar to World War II and Korea. In the past a major engineering problem in weapon system design has been the lack of knowledge concerning penetration mechanics. Throughout history research into this subject area has stopped when hostilities cease. The mechanism of penetration has therefore never been fully explained. Although many shots have been fired under carefully controlled conditions, there is no satisfactory model of the perforation. The deformation and failure of plates have been characterized empirically many times. The results have generally led to an equation relating size and shape of the projectile, thickness of the plate, and the impact velocity. The modern day aircraft, vulnerable to small arms and fragment penetration due to thin skin, high speed, high engine temperatures, and volatile fuel, has given the Air Force renewed interest in this aspect of airplane design. The object of this investigation is, therefore, to describe one aspect of the impact mechanism; specifically, the flash of light resulting from the impact of high-speed fragment simulator projectiles on thin aluminum plates. The temperature and duration of the flash are the primary

areas of interest.

Background

One of the first extensive investigations of impact flash phenomena was made by Norman Brown (Ref 7) in 1948. His method involved estimates from still pictures and use of a high-speed framing camera to determine time sequence and duration. In 1952 R. L. Kahler (Ref 19:1-7) observed that an inert atmosphere reduced the impact flash, and that pure oxygen enhanced the flash. His results confirmed Brown's finding that reduced pressure reduced the flash. In 1952 Roland G. Bernier (Ref 4) conducted a series of tests with various target and projectile combinations. His findings related projectile mass, density, and velocity to the flash size and duration. In 1955 W. T. Thompson (Ref 33:80) published a report on armor penetration in which he suggested that the target projectile interface was molten. The existence of the molten interface formed the basis for R. F. Recht's theory of impact failure, which he called "Catastrophic Thermoplastic Shear". (Ref 29:189) He proposed that failure occurred when the local rate of change of the temperature had a negative effect on strength which was equal to or greater than the positive effect of strain hardening. Joseph M. Krafft (Ref 23:1249) conducted a series of experiments to estimate the percentage of projectile striking energy that was absorbed by sliding friction. He found that for "mechanically" clean surfaces the

friction accounted for 3% of the energy loss, but ordinary handling introduced enough lubricant to reduce the loss to less than 1%. In 1960 D. D. Keough (Ref 20) used a photomultiplier system to detect flashes from microparticles at higher velocities. His work was an indication of the shift in emphasis to space application and micrometeorite particle detection. He reported that reduced atmospheric pressure resulted in longer rise times for the flash luminosity although other descriptors remained unchanged. The more recent investigations have been primarily concerned with space applications and hence, have usually been in the hypervelocity range. In 1964 F. W. MacCormack (Ref 24) made a thorough investigation of the impact flash at hypervelocities and low ambient pressure. He concluded that microscopic particles of ejecta emerge, and due to high-speed aerodynamic effects heat, ablate, and radiate in the manner of meteors. A. P. Caron (Ref 10) suggested that the pyrophoric oxidation reactions of the impacted projectile and target material with gaseous oxygen were the cause of the luminosity. He used the ideas of Bull (Ref 9) and Bjork (Ref 5) to show that the impact compressed the target and projectile to high pressures and temperatures. The "excited" ejecta particles were thrown into the gaseous oxygen where oxidation could take place with the finely dispersed metal.

Backman and Stronge (Ref 2) have recently (1967) correlated luminosity with the vapor-phase-combustion pro-

GAW/MC/68-1

cess. Their conclusions are similar to those of MacCormack; the high speed flow causes the material ejecta to heat and ablate, and then burn in the oxygen atmosphere.

II. Physical Model

The overall physical model of the flash can be divided into three phases. The material must be removed from the plate by the rupture phase. Then, because of high speeds the particles are heated, and the surfaces melt and flow during the ablation phase. Finally, the exposed surface area and the oxygen available in the atmosphere combine chemically giving the burning phase.

Rupture Phase

Thompson's discussion of a dynamical approach to armor penetration (Ref 33), Krafft's experiments on friction (Ref 23), and Recht's thermoplastic shear (Ref 29) have presented careful documentation for increased temperatures in the particles being ejected by a ballistic impact. Although the velocities of this investigation do not qualify as hypervelocity, the qualitative arguments of Bjork and Olshaker (Ref 5) certainly are applicable in that the material has been shocked to a higher energy state and during the recovery retains a percentage of that energy. There can be little doubt that the particles torn from the target plates during the impact are at an increased temperature. The discussion by Rinehart (Ref 31) of spalling and scabbing indicates a mechanism for thrusting excited particles into a stream of down range ejecta.

Ablation Phase

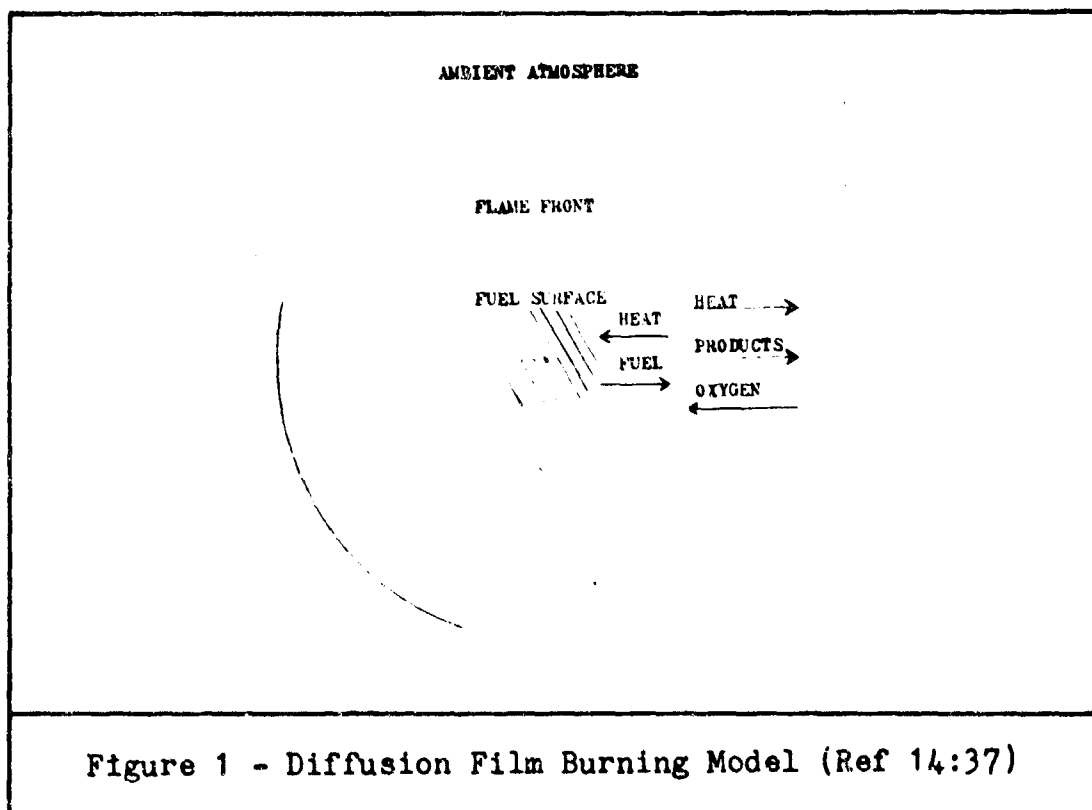
The ignition of the particles is most likely a surface burning phenomena (Ref 14:20). If the particles are subjected to high speed flow, the surrounding gas envelope would melt the material and hence ablate, continuously exposing new surface area and also providing smaller particles or droplets for the burning phase.

Burned Ejecta Phase

T. H. Rautenberg and P. D. Johnson (Ref 28) investigated the characteristics of the Aluminum-Oxygen reaction in flashbulbs. By comparing the spectral lines of aluminum and sodium; known to be in thermal equilibrium with the other degrees of freedom in flames (Ref 13:169), they concluded that since all the temperatures observed were essentially the same, the AlO system was excited thermally rather than directly by the arc. The enhanced energy production by aluminum powders in explosives and rocket fuels led to extensive investigation of the mechanism of reaction. Irvin Glassman (Ref 14), R. W. Bartlett, et al (Ref 3), Andrej Maček (Ref 25), and Thomas Brzustowski (Ref 8) were primary workers in the field. The ultimate model for combustion appears to be a diffusion controlled flame front surrounding the solid or liquid metal core. (see Figure 1). Brewer and Searcy (Ref 6) investigated the $Al - Al_2O_3$ system in an effusion cell, and from the vapor pressure measurements they obtained a boiling point of $3800^{\circ} \pm 200^{\circ}K$

GAW/MC/68-1

for Al_2O_3 . Glassman asserted (Ref 14:5) that the boiling point of the oxide might be taken as the combustion temperature. Aluminum is in the category of metals which have a vaporization temperature for the oxide ($3800^{\circ}K$) greater than the vaporization temperature for the pure metal ($2720^{\circ}K$), and hence it follows the model of Figure 1.



III. Spectroscopic Temperature Measurement

Theory

The intensity of spectral line structure in emission, I_{em}^{nm} , is defined as the energy emitted by the source per second. If there are N_n atoms in the initial state, and if A_{nm} is the fraction of atoms in the initial state carrying out the transition to m per second then:

$$I_{em}^{nm} = N_n h c \nu_{nm} A_{nm} \quad (1)$$

where $h c \nu_{nm}$ is the energy of each light quantum of wave number ν_{nm} emitted in the transition. A_{nm} is the Einstein transition probability of spontaneous emission and is given as:

$$A_{nm} = \frac{64\pi^3 \nu_{nm}^3}{3h} \left| \vec{R}_{nm} \right|^2 \quad (2)$$

(Ref 1; 7-176)

where \vec{R}_{nm} (transition moments) are the matrix elements of the electric dipole moment \vec{M} of the system.

The term "band spectrum" is used to designate a spectrum which originates from either emission or absorption in the molecules of a compound. The intensity of band system structure depends on three things: (1) the frequency ν , (2) the number of molecules in the initial state, and (3) the transition probability.

Frequency

The energy associated with a molecule may be separated into three elements which are: (1) electronic, due to changes in outer electronic structure; (2) vibrational, due to vibration of the component atoms relative to each other; and (3) rotational, due to rotation of the molecule as a whole about the center of gravity. To indicate the division of energy in molecular spectra, the wave number or term value expression is usually given: $T = T_e + G + F$ where:

T_e = electronic term value

G = vibrational term value

F = rotational term value

When discussing a particular transition, $\nu' \rightarrow \nu''$, the wave number corresponding to the transition is given by:

$$\nu = T' - T'' = (T_e' - T_e'') + (G' - G'') + (F' - F'') \quad (3)$$

or

$$\nu = \nu_e + \nu_v + \nu_r \quad (4)$$

For a given electronic transition ν_e is a constant representing the difference between the two minima of the energy states; and since, in general, F is small compared to G ,

$\nu_r = (F' - F'')$ may be neglected. These simplifications result in a coarse structure of the electronic transition which may be called the vibrational structure since ν_v is the only variable. Hence the form of the wave number expression is:

$$\nu = \nu_e + \omega_e (v + \frac{1}{2}) - \omega_e x_e (v + \frac{1}{2})^2 + \dots - \left[\omega_e (v + \frac{1}{2}) - \omega_e x_e (v + \frac{1}{2})^2 + \dots \right] \quad (6)$$

where:

ω_e = vibrational frequency (cm)

$\omega_e x_e$ = amplitude of first overtone or second harmonic

and $\omega_e x_e \ll \omega_e$, as are all coefficients on successive terms in the two expansions. Since there are no strict selection rules for vibrational quantum numbers, equation (5) represents all possible transitions between the different vibrational levels of the two participating electronic states.

Population

The distribution of molecules may be determined from the Maxwell-Boltzmann law when thermal equilibrium exists. Since only discrete values of vibrational energy are possible, the number of molecules in each of the vibrational states is proportional to the Boltzmann factor

$$\exp[-E/kT]$$

where:

$E = G(v) hc$

$G(v)$ = vibrational term value (cm^{-1})

h = Planck's constant (6.623×10^{-27} erg-sec)

c = speed of light in vacuum (2.998×10^{10} cm/sec)

k = Boltzmann's constant (1.38033×10^{-16} erg/degree)

T = absolute temperature (degrees Kelvin)

The quantity $\exp[-G(v)hc/kT]$ gives the relative number of molecules in each vibrational level referred to the number of molecules in the lowest vibrational level. The total number of molecules N is proportional to the sum of the Boltzmann factors over all states, (the partition function).

$$Q_v = 1 + \exp[-G(0)hc/kT] + \exp[-G(1)hc/kT] + \dots \quad (6)$$

Therefore, the number of molecules in the state v' is

$$N_{v'} = \frac{N}{Q_v} \exp[-G(v')hc/kT] \quad (7)$$

Transition Probability

The Franck-Condon principle for emission relates the transition probability to band intensity. According to the principle, (Ref 37:315) electronic transitions to lower energy states take place at constant internuclear distance (i.e. vertical lines in Figure 2). In order to avoid a discontinuity in velocity the lower state selected must also be one with the same turning point location.

So:

$$I_{em}^{v'v''} = \frac{64\pi^4}{3} c \nu_{v'v''}^4 N_{v'} \overline{R_e}^2 \left[\int \psi_{v'} \psi_{v''} dr \right] \quad (8)$$

By properly normalizing the orthogonal eigenfunctions, the sum of the squares of the integrals for all transitions can be shown to be equal to one (Ref 16:203). By summing over all transitions and rearranging, equation (8) becomes:

$$\sum \frac{I_{em}^{v'v''}}{\nu_{v'v''}^4} \propto N_{v'} \quad (9)$$

Then, equating this sum to the population (Boltzmann distribution) and taking the logarithm gives:

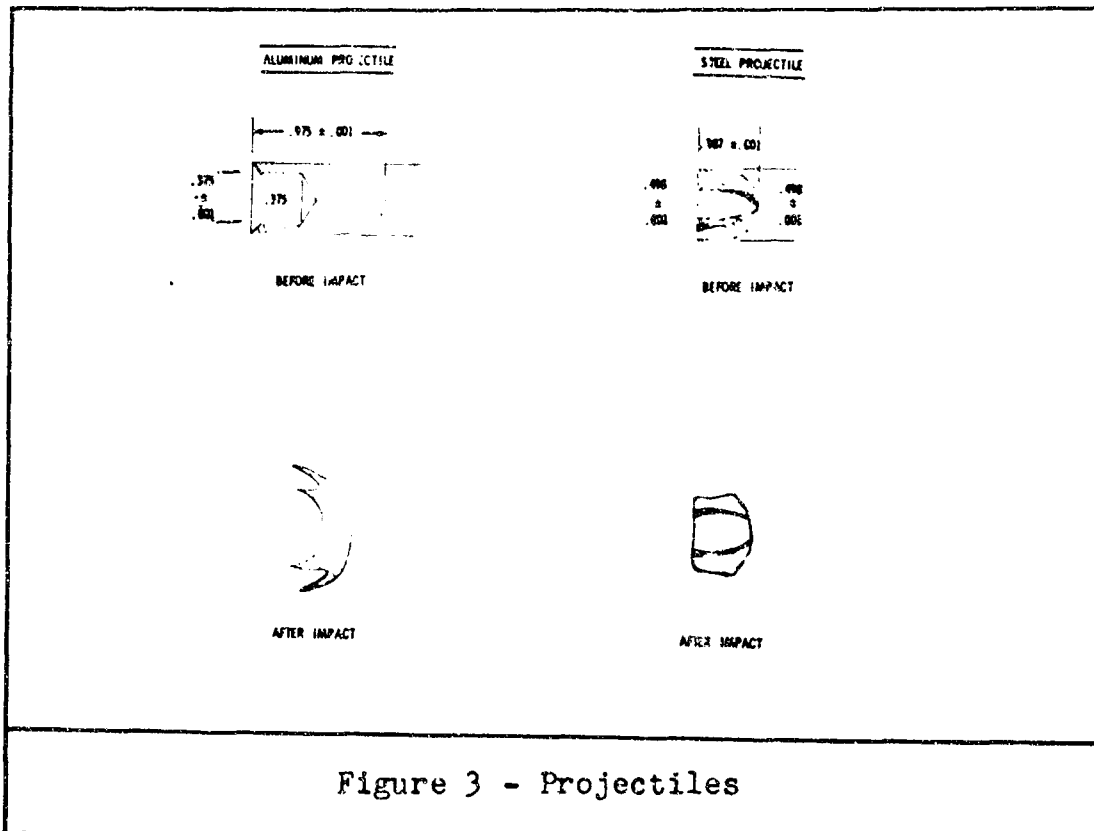
$$\log \left[\sum \frac{I_{em}^{v'v''}}{\nu_{v'v''}^4} \right] \propto C_1 - \frac{G(v') h c}{kT} \quad (10)$$

$C_1 = \text{Constant}$

where the quantity $\frac{I_{em}^{v'v''}}{\nu_{v'v''}^4}$ is called the band strength. By plotting the log of the sums of band strengths, as measured in the ν'' progressions ($\nu' = \text{constant}$); against the vibrational term values $G(v')$ times the constants a straight line with slope $(-\frac{1}{T})$ is obtained.

IV. Experimental Method

Since several investigators (Ref 2, 10, 35) have indicated that a minimum velocity is necessary to cause an impact flash, it was decided to use the maximum velocity consistently attainable with a powder load of 240 grains of Dupont 3031. The amount of powder did not completely fill the cartridge, so one and a half cleaning patches were used to fill the void and keep the powder density uniform. The neck on the cartridge was resized between shots, and a crimp ring was pressed into the neck so that the projectile would rest at a common position for each loading. See Appendix A for range layout and equipment. The velocities attained fall essentially into two groups, one for the steel projectiles and the other for the aluminum. The difference in velocity is due to the difference in mass of the two projectile types. The mean steel projectile was 115.4 grains with a standard deviation of 2.78 grains, and the mean aluminum projectile was 82.2 grains with a standard deviation of 2.12 grains. See Figure 3 for projectile dimensions. The projectiles were designed with a hemispherical nose so that effects of small variations from normal impact on impact flash were minimized.



A spectrograph, photomultiplier system, streak camera, and image converter camera were used to record the overall view, spectral response, and time history of the impact flash.

The image converter camera could be used to develop a sequence of three exposures for each event. The delay between exposures and the exposure time was adjusted so that various intensity levels were observable. The usual method employed was to limit the exposure time and aperture to the minimum in an effort to penetrate as far as possible into the luminous cloud core.

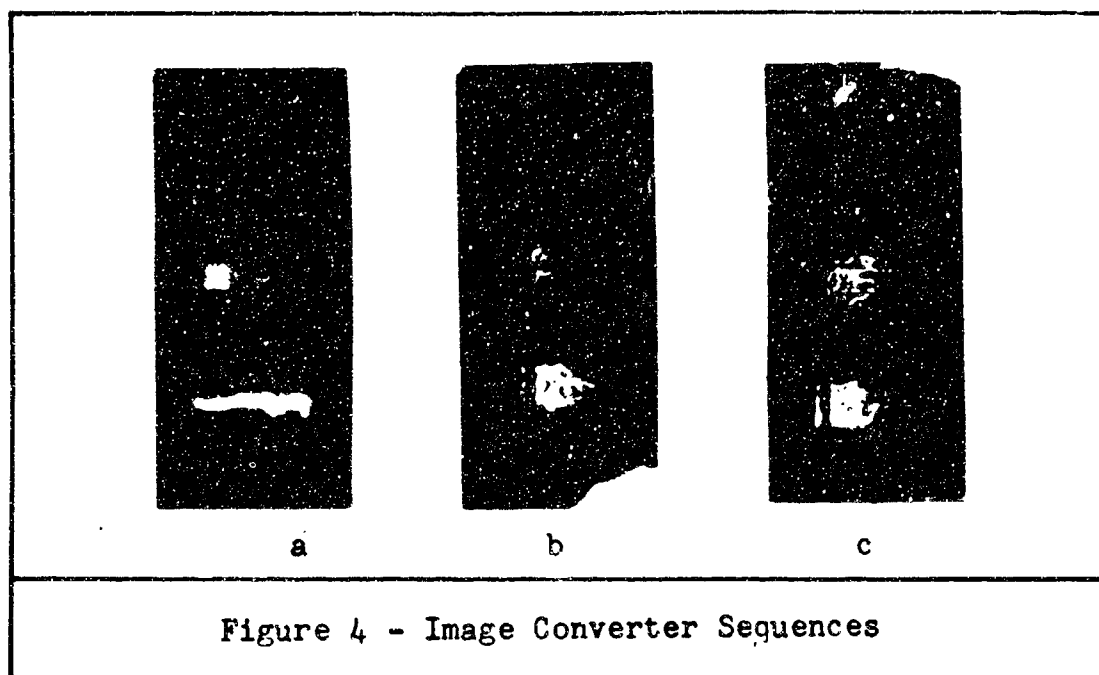


Figure 4a,b,c show the results from experiments A10, A15, and A23 respectively. The projectile was traveling from left to right with an f11 lens setting; the exposure sequences (top to bottom) are listed in Table I.

	Delay (microseconds)	Exposure (microseconds)
1	15	2
2	10	2
3	20	1

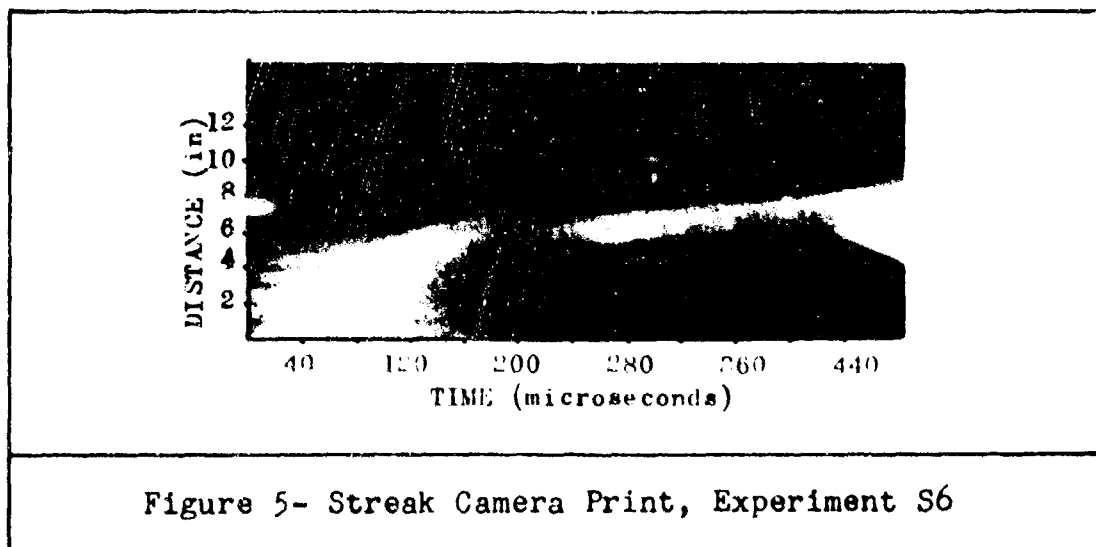
Image Converter Sequences

Table I

The photomultiplier-optical system was intended to record the total radiation of the impact flash. The manufacturer reported the rise time of the system as 3 milli-

microseconds, so it was felt that there would not be any difficulty in recording the event. The output of the photomultiplier system was the input for a single sweep, two time base oscilloscope. The sweep rates were adjusted so that one trace concentrated on the rise portion of the curve and the other recorded the entire event. The optical viewfinder system made it possible to accurately align the photomultiplier with the intended impact point.

A distance vs. time picture of the event was produced by locating a streak camera so that the film and projectile were moving on mutually perpendicular axes. One milli-second interval timing marks were used to calculate the film speed, and a reflective tape grid was positioned to give down range distance information. Failure to move down range was indicated by a streak parallel to the long axis of the film. In addition, variations in intensity also were recorded by the streak camera (See Figure 5).



The photographed grid system was used to calculate distances traveled down range, and the time marks were used to calibrate the long axis of the film so that accurate readings of distance and time could be taken. AFIT Aid Program 225 was used to generate a 2nd order polynomial fit for the co-ordinates taken from the photographs. The velocity at selected points could be determined by evaluating the derivative at the desired location.

The spectrograph was focused on the intended impact point. The field of view extended a distance of 1.6 inches along the projectile line of flight axis when the spectrograph slit was 16 inches from the impact aim point. (See Figure 6).

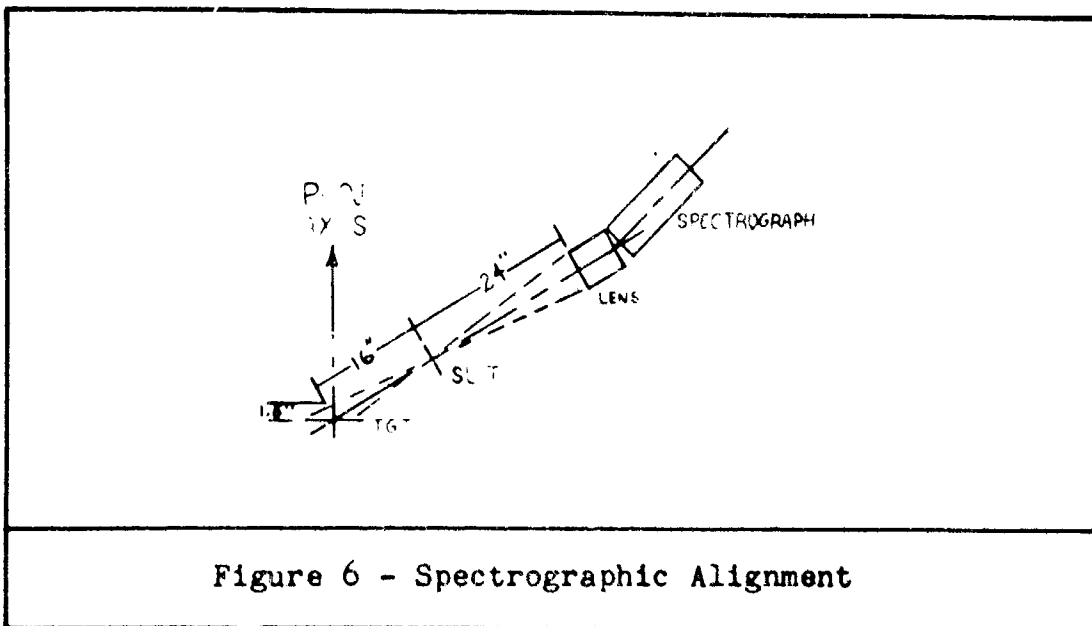
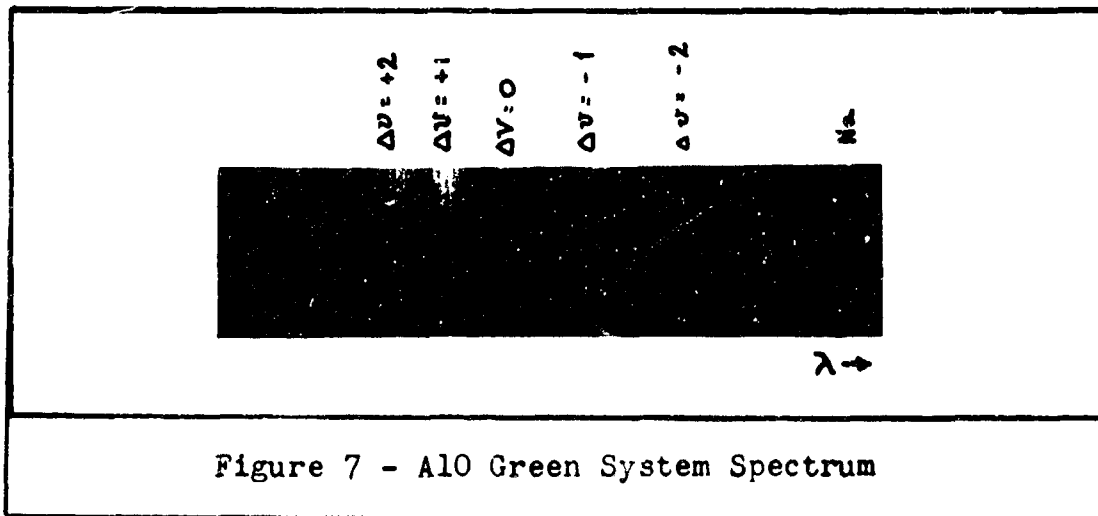


Figure 6 - Spectrographic Alignment

The time integrated spectral response was recorded for each shot. The film was carefully developed, and useful film records were measured on a Jarrell-Ash 21-050 micro-

photometer with a Bristol Dynamaster Recorder. The microphotometer record was translated into intensity using the method developed by Johnson and Tawde (Ref 17:580). See Appendix B for film calibration procedure. The readings were then tabulated and processed through the IBM 1620 computer using the program in Appendix C. Figure 7 is a print from experiment A19 showing the A10 green system.



V. Results

Tables II and III list the experimental results by projectile type; and tabulate weight, velocity, target (material and thickness), hole diameter, and the ratio of hole area to projectile area. The ratio of hole area to projectile area is plotted against the ratio of target thickness to projectile diameter in Figure 8.

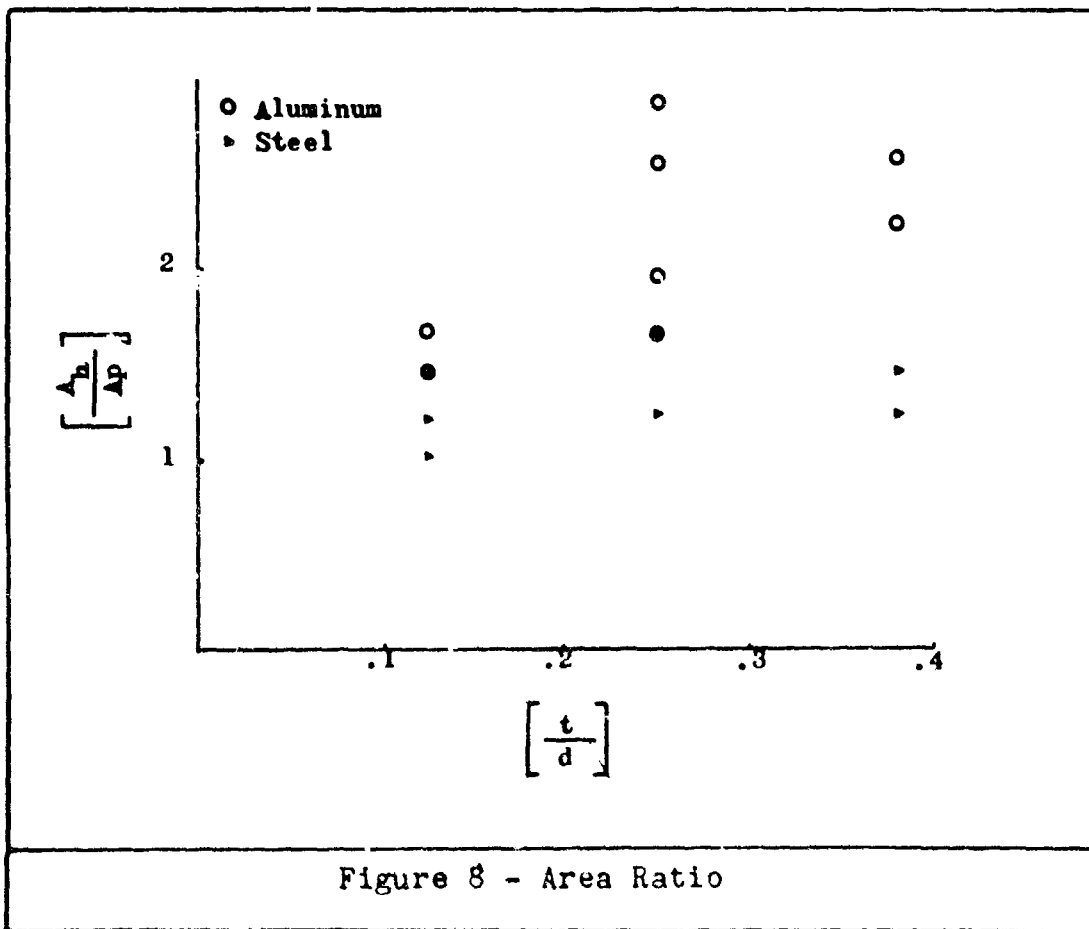


Figure 9 is a typical result of streak camera interpretation, and Table IV gives the luminous cloud velocity at selected time intervals. The spectrographic data are pre-

GAW/MC/68-1

sented in Figure 10; the lines were determined by the method of least squares. The mean value and standard deviation are indicated for each term value. The relative intensity values for a typical shot are presented in Table V.

Shot No.	Weight (grains)	Velocity (ft/sec)	Material	Thickness (inches)	Hole Dia. (inches)	$\frac{\text{Area}_H}{\text{Area}_P}$
A 1	85.2	4680	2024 T-3	0.063	0.65	1.69
A 2	79.8	4710	2024 T-3	0.063	0.60	1.44
A 3	80.0	4710	2024 T-3	0.063	0.60	1.44
A 4	81.1	4670	2024 T-3	0.063	0.60	1.44
A 5	81.1	4690	2024 T-3	0.063	0.65	1.69
A 6	79.8	4710	2024 T-3	0.063	a	b
A 7	79.5	4720	2024 T-3	0.063	a	b
A 8	80.4	4690	1100	0.063	0.65	1.69
A 9	81.0	4740	1100	0.063	0.60	1.44
A 10	83.7	4700	7075 T-6	0.063	0.60	1.44
A 11	84.7	4710	7075 T-6	0.063	0.65	1.69
A 12	86.0	4780	7075 T-6	0.063	0.60	1.44
A 13	84.6	4760	7075 T-6	0.063	0.65	1.69
A 14	80.7	4730	1100	0.125	0.80	2.56
A 15	80.8	4690	1100	0.125	0.85	2.89
A 16	80.6	4780	1100	0.125	0.70	1.96
A 17	80.0	4630	1100	0.125	0.80	2.56
A 18	80.3	4900	1100	0.125	0.80	2.56
A 19	83.2	5050	2024 T-3	0.125	0.80	2.56
A 20	84.8	4800	2024 T-3	0.125	a	b
A 21	80.0	5010	7075 T-6	0.125	0.70	2.89
A 22	80.6	4760	7075 T-6	0.125	0.70	2.89
A 23	85.0	4850	2024 T-3	0.190	0.75	2.25
A 24	84.5	4780	2024 T-3	0.190	0.80	2.56
A 25	79.8	4910	2024 T-3	0.190	0.75	2.25
A 26	83.8	4910	2024 T-3	0.190	0.75	2.25
A 27	84.6	5040	2024 T-3	0.190	a	b
A 28	80.7	4960	7075 T-6	0.190	0.80	2.56
A 29	83.2	4880	7075 T-6	0.190	0.75	2.25
A 30	80.4	4940	7075 T-6	0.190	0.75	2.25
A 31	84.3	4570	7075 T-6	0.190	0.75	2.25
A 32	80.8	4760	7075 T-6	0.190	0.75	2.25

a - Not measured

b - Not calculated

Aluminum Projectile Data

Table II

Shot No.	Weight (grains)	Velocity (ft/sec)	Material	Thickness (inches)	Hole Dia.	$\frac{Area_h}{Area_p}$
S 1	121.7	4360	1100	0.063	0.55	1.21
S 2	120.6	4330	1100	0.063	0.55	1.21
S 3	115.2	4580	1100	0.063	0.50	1.00
S 4	115.2	4560	1100	0.063	0.55	1.21
S 5	115.5	4470	2024 T-3	0.063	0.50	1.00
S 6	115.6	4490	2024 T-3	0.063	0.55	1.21
S 7	120.3	4330	7075 T-6	0.063	0.60	1.44
S 8	116.1	4540	7075 T-6	0.063	0.50	1.00
S 9	114.3	4590	1100	0.125	0.65	1.69
S 10	114.1	4460	1100	0.125	0.65	1.69
S 11	116.5	4450	1100	0.125	0.65	1.69
S 12	118.5	4360	1100	0.125	0.65	1.69
S 13	a	4450	2024 T-3	0.125	0.55	1.21
S 14	a	4450	2024 T-3	0.125	0.55	1.21
S 15	116.7	4330	2024 T-3	0.125	0.55	1.21
S 16	112.0	4440	7075 T-6	0.125	0.55	1.21
S 17	112.8	4460	7075 T-6	0.125	0.50	1.21
S 18	112.6	4450	2024 T-3	0.190	0.60	1.44
S 19	112.0	4510	2024 T-3	0.190	0.60	1.44
S 20	113.1	4400	2024 T-3	0.190	0.60	1.44
S 21	113.0	4450	2024 T-3	0.190	0.60	1.44
S 22	113.8	4440	7075 T-6	0.190	0.55	1.21
S 23	a	4500	7075 T-6	0.190	0.55	1.21
S 24	a	4580	7075 T-6	0.190	0.55	1.21
S 25	114.5	4370	7075 T-6	0.190	0.60	1.44
S 26	113.7	4400	7075 T-6	0.190	0.60	1.44

a - Not measured

Steel Projectile Data

Table III

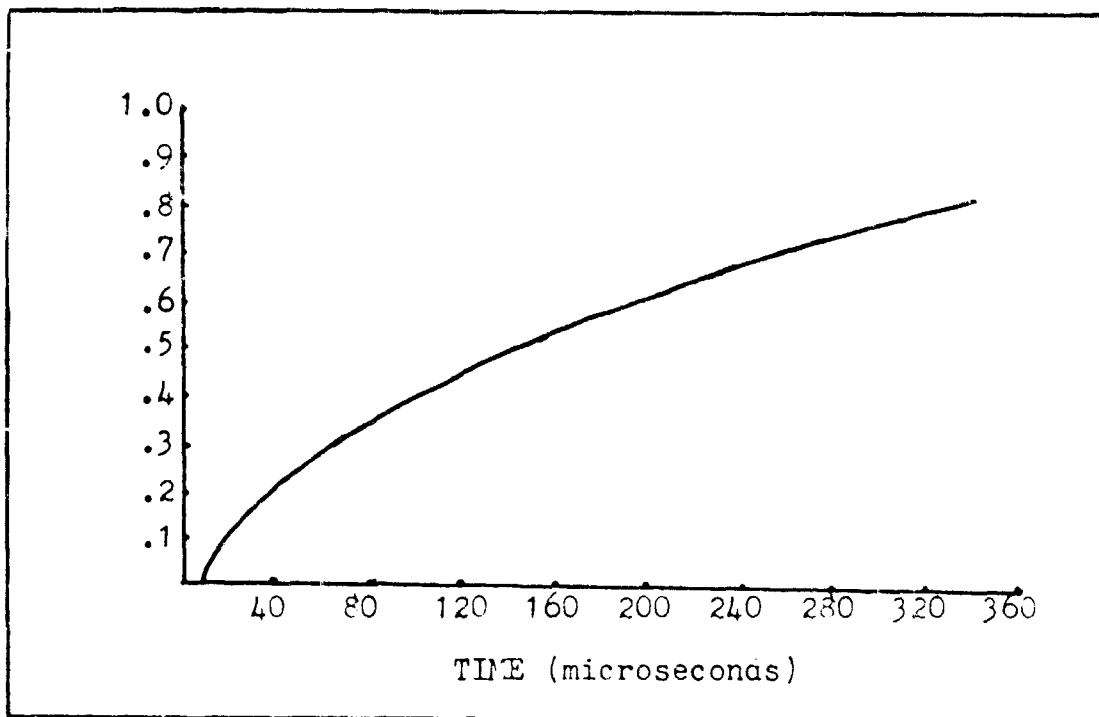
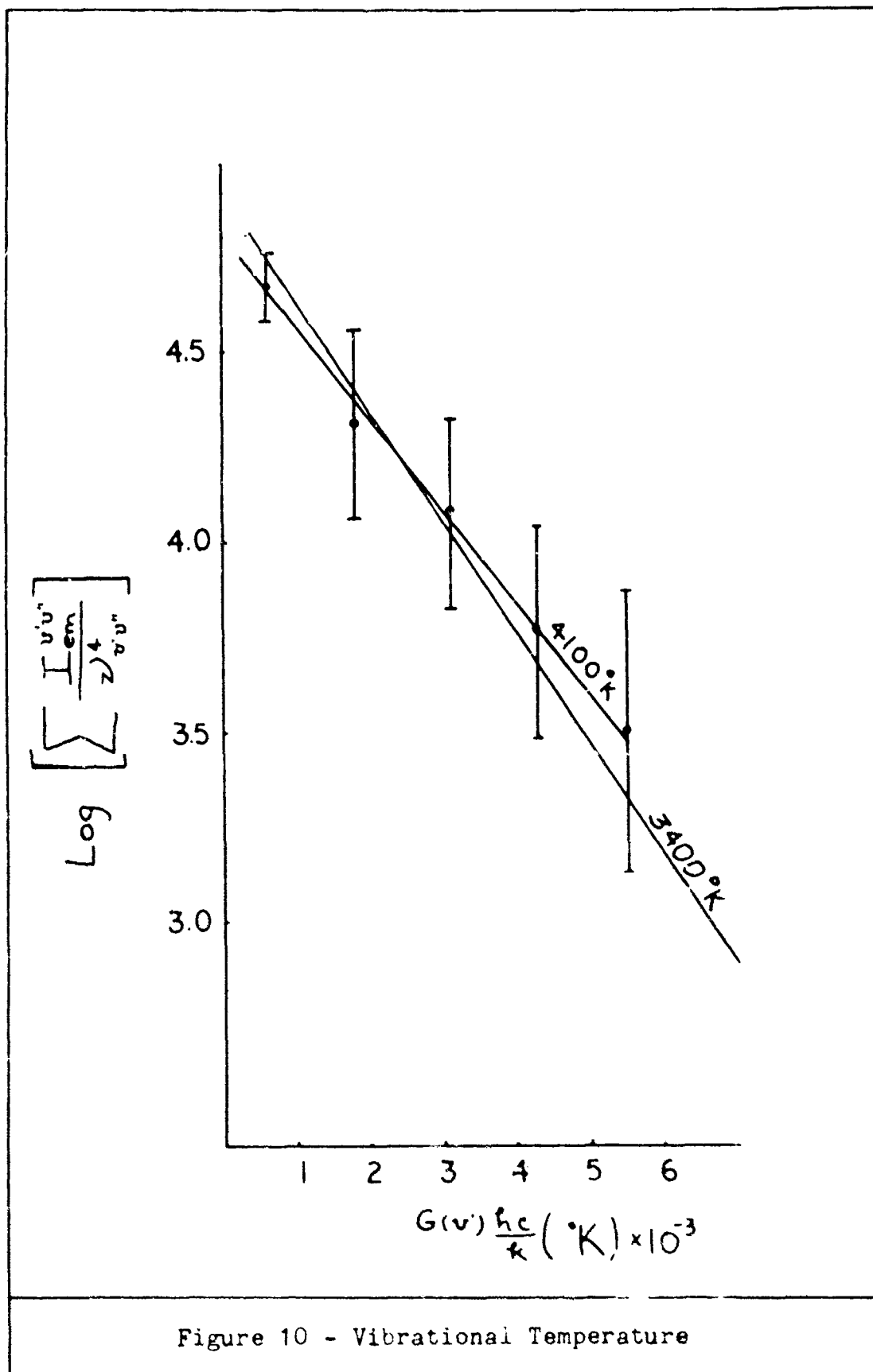


Figure 9
Time Distance Trace From Least Squares Fit Experiment S 6

Position (feet)	Velocity (ft/sec)
0.1	7537
0.2	4533
0.3	3241
0.4	2522
0.5	2064
0.6	1747
0.7	1514
0.8	1336

Down Range Velocity

Table IV



INTENSITY

V ⁿ	0	1	2	3	4	5	6
0	100.00	45.95	10.81	0.00	0.00	0.00	0.00
1	16.22	21.62	35.14	16.22	0.00	0.00	0.00
2	32.43	51.35	18.92	2.70	10.81	0.00	0.00
3	0.00	16.22	32.43	0.00	21.62	10.81	0.00
4	0.00	0.00	18.92	27.03	0.00	21.62	13.51
5	0.00	0.00	0.00	21.62	10.81	0.00	16.22
6	0.00	0.00	0.00	0.00	16.22	0.00	0.00

Relative Intensity Table for Experiment A18

Table V

The photomultiplier trace (See Figure 11) is for experiment S19; the upper trace was on 1 cm/.5 milliseconds, and the lower trace was set for 1 cm/50 microseconds.

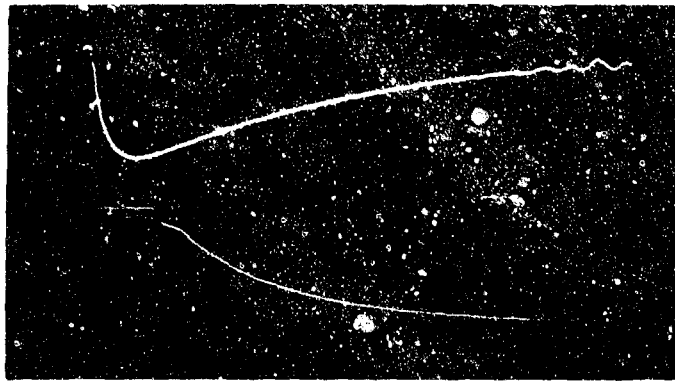


Figure 11 - Photomultiplier Trace

VI. Discussion of Results and Conclusions

Due to the difference in projectile mass, the velocities attained were separated into two groups. The mean velocity for the steel projectile was 4452 fps with a standard deviation of 78 fps, and for the aluminum projectiles was 4788 fps with a standard deviation of 121 fps. The aluminum projectiles consistently caused a larger hole in the target plate. The most probable reason was the gross deformation of the aluminum projectile during the perforation process. See Figure 3 for a recovered projectile shape. Olshaker (Ref 26) has plotted $\left[\frac{A_h}{A_p} \right]$ against the ratio of target thickness to projectile diameter $\left[\frac{t}{d} \right]$. His information, although for a higher velocity and for different materials, indicates a linear increase in $\left[\frac{A_h}{A_p} \right]$ with target thickness. The decrease in hole area with diminishing sheet thickness can be explained by the physical model of thin plate perforation, which indicates that the hole size is smaller in the thinner target due to a quicker reduction of shock strength caused by the weakening effect of the rarefaction from the rear of the target, which in turn leads to a smaller impulse per unit of lateral area (Ref 18:21).

The Rockwell hardness of the steel projectiles was approximately C54 prior to the impact and B10 afterward. An attempt was made to examine the microstructure of the

steel, but no changes were detectable except for some cracks in the rear half of the projectile generally parallel to the longitudinal axis.

The scatter in perforation data may be attributed to errors in measurement of the hole diameter. An attempt was made to measure to the nearest 0.05 inches at the smallest dimension. See Figure 12.

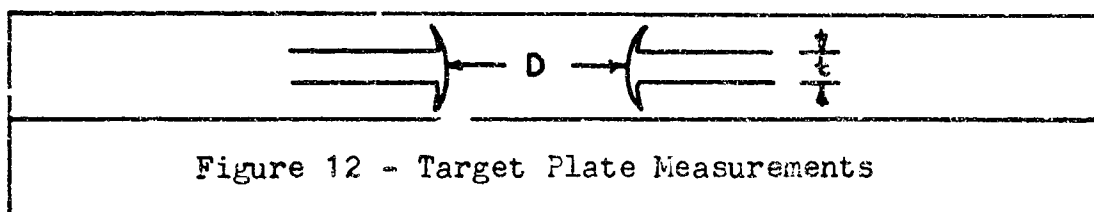


Figure 12 - Target Plate Measurements

It was felt that due to asymmetries there would be no value in trying to measure with more precision. This could lead to an error of approximately 12% in area calculations. The area for all projectiles was taken as 0.196 square inches, which would underestimate the area of a deformed projectile.

The overall dimensions of the flash varied considerably. The length is estimated to be 14 inches and the maximum transverse dimension approximately five inches. (See Figure 13a,b).

posures even though the impact point was not as accurate as for the steel projectiles. The increased success rate can be attributed to the additional availability of oxygen to react with the freshly exposed aluminum surfaces.

An unsuccessful attempt was made to measure the effect of nitrogen on the flash. A qualitative examination of the still pictures indicated that the system did not suppress the flash. This may be attributed to a latent gaseous oxygen content of approximately 6% at the time of the impact. These results indicate that although increased oxygen availability enhanced the impact flash, the removal of oxygen to suppress the flash would require more thorough purging.

The results of the spectrographic analysis given in Figure 10 indicate that the effective vibrational temperature (from the AlO green system) is 4100°K . As can be seen by the increasing separation of the data, the higher term values are more difficult to locate and interpret. Herzberg (Ref 16:204) points out that the success of the "sum rule" method of temperature determination depends on two things; first, measuring all of the bands in the progressions used, and second, the source has to be in thermal equilibrium. Tawde (Ref 32:734) reported that there were 34 bands of the AlO system. His data (Appendix C, Table VI) included the sequence $\Delta\nu = +3$. Apparently the equipment used in this investigation was not sensitive enough to distinguish this sequence. Failure to include this term would

lower the sum for progressions after the third term value. Figure 10 shows the least squares fit for the first three term value points, and also, the fit for the entire collection of data. The temperature (read directly as the slope of the curve) for the entire collection of data was 3400°K , and the value for the first three terms is 4100°K . The 4100°K temperature is identical to that reported by Backman (Ref 2:38) and the 3400°K corresponds to the findings of Tawde (Ref 32:734) for an AlO system excited by a carbon arc. These values also bracket the $3800^{\circ+}200^{\circ}\text{K}$ (Ref 6:5308) for the vaporization temperature of Al_2O_3 at atmospheric pressure. The vaporization temperature was suggested by the model (See Section II), and the reported bounds indicate that these values should be considered as reasonable estimates for the flame temperature.

Since there was no spectroscopic evidence of anything but AlO and sodium, (a contamination) it was decided to lump all the data points including the steel projectile before computing the least squares fit.

The limited field of view restricted the use of the photomultiplier system to qualitative information about the flash. The shock in the range area induced microphonics in the recording equipment, which caused spurious output signals. Kottenstette (Ref 21:25) had reported that he detected different time histories for different bands of the AlO system. The broad spectral response characteristics (S20) of the photomultiplier system did not allow selective

band investigation.

In conclusion, the results of this investigation indicate that the impact flash produced by cylindrical projectiles with hemispherical heads on thin aluminum targets lasts approximately 3-5 milliseconds. The dimensions of the flash were found to be approximately 14 inches by 5 inches. The effective vibrational temperature, determined from the A10 green system, was found to be between 3400° and 4100°K . These temperatures agree with previously reported information (Ref 2:32) and are compatible with the physical model.

VII. Recommendations

The analysis of this investigation has led to several recommendations.

a. A more efficient light gathering system is necessary. Friend et al (Ref 11:37) used a reflector slightly offset from the projectile axis to gather light and focus on the entrance for a spectrograph.

b. A method of fixing calibration and time resolution on each spectrographic record is highly desirable.

c. High speed framing camera results would be helpful in relating all data to a common base.

d. A flash X-ray is desirable in order to determine projectile integrity and ejecta spray pattern.

e. The Hy-Cam rotating drum camera (available through Tech Photo) might effectively be employed to record the variations in spray pattern ejecta and light intensity.

f. Although a filtered photomultiplier system would be more difficult to assemble, the results could be continuously monitored and recorded.

Bibliography

1. American Institute of Physics Handbook (Second Edition), McGraw Hill, New York, 1963.
2. Backman, M. E. and W. J. Stronge. Penetration Mechanics and Post-Perforation Effects in an Aluminum-Aluminum Impact System. NWC-TP-4414. China Lake, California, 1967.
3. Bartlett, R. W. et.al. Estimating Metal Particle Combustion Kinetics. Aeronutronic Report U-1751. Newport Beach, California: Ford Motor Company, July, 1962.
4. Bernier, R. G. Aluminum and Magnesium Fragments vs. Dural Plates. Unpublished report from BRL, Aberdeen, Maryland. October, 1952.
5. Bjork, R. L. and A. E. Olshaker. The Role of Melting and Vaporization in Hypervelocity Impact. The Rand Corporation RM - 3490 - PR, May, 1965.
6. Brewer, L. and A. W. Searcy. J. A. C. S. 73 (1951) 5308.
7. Brown, N. Size and Duration of Sparks Produced by Impact of Steel and Pyrophoric Simulated Fragments on Thin Metal Plates. BRL R - 683. Aberdeen, Maryland. December, 1948.
8. Brzustowski, T. A. and I. Glassman. "Vapor Phase Diffusion Flames in the Combustion of Magnesium and Aluminum", in Heterogeneous Combustion (Progress in Astronautics and Aeronautics). Edited by Hans G. Wolfhard, et.al. 15: Academic Press, 1964. 75-158.
9. Bull, G. V. et.al. "Review of Hypervelocity Impact Studies at McGill University." Report 63-15, NASW-615, December, 1963.
10. Caron, A. P. Oxidative Detonations Initiated by High Velocity Impacts. AFFDL - TR - 65-41, May, 1965.
11. Friend, W. H., et.al. An Investigation of Explosive Oxidations Initiated by Hypervelocity Impacts. AFFDL-TR - 67-92. Wright-Patterson Air Force Base, Ohio: Air Force Flight Dynamics Laboratory, May, 1967.

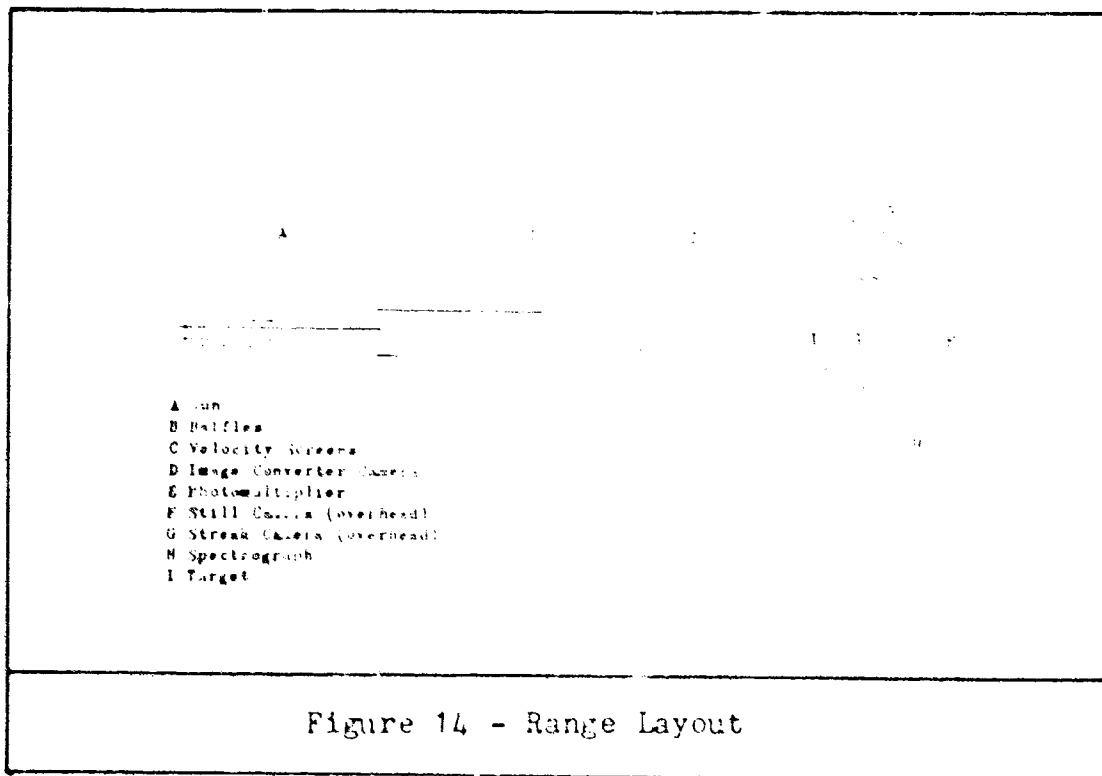
12. Fruchtenicht, J. F. Experiments on the Impact-Light-Flash at High Velocities. NASA - CR - 416. Washington: National Aeronautics and Space Administration, March, 1966.
13. Gaydon, A. G. Spectroscopy and Combustion Theory. London: Chapman and Hall Ltd., 1948.
14. Glassman, Irvin. Metal Combustion Processes. New York: Paper presented to American Rocket Society, 14th Annual Meeting, Washington, November, 1959.
15. Harrison, G. R. et.al. Practical Spectroscopy. Englewood Cliffs, New Jersey. Prectice-Hall, 1948.
16. Herzberg, G. Molecula Spectra and Molecular Structure. (Second Edition) Princeton: D. Van Nostrand Co., 1950.
17. Johnson, R. C. and N. R. Tawde. "Intensity Distribution in Molecular Spectra." Proceedings of the Royal Society of London, A 137: 575-591., September, 1932.
18. Jones, A. H. et. al. Survey of Hypervelocity Impact Information II. ASRL Report 99-2. MIT: December, 1963.
19. Kahler, R. L. Impact Flash Suppression. Joint USAF-USN Technical Symposium on Aircraft and Missile Vulnerability. Wright-Patterson Air Force Base: September, 1952.
20. Keough, D. D. Luminosity Studies of High Velocity Impact. AFCRL - TR - 60-415. Bedford, Massachusetts. October, 1960.
21. Kottenstette, J. P. Impact Flash Characteristics of Triboluminesent Material. AFTL - TR - 65-75: Eglin Air Force Base, November, 1965.
22. Kottenstette, J. P. and E. Wittrock. Impact Flash Characteristics as Affected by Oxidizing Materials. AFATL - TR - 67-2. Eglin Air Force Base, February, 1967.
23. Krafft, J. M. "Surface Friction in Ballistic Penetration". Journal of Applied Physics, 26: 1955. 1248-1252.
24. MacCormack, R. W. Impact Flash at Low Ambient Pressures. NASA TN D - 2232. Washington: National Aeronautics and Space Administration. March, 1964.

25. Macek, A. and J. McKenzie Semple. Time Resolved Spectroscopy of Single Burning Metal Particles. Project Solid Technical Report ARC - 10 - P. Charlottesville, Virginia: University of Virginia, June, 1966.
26. Olshaker, A. "An Experimental Investigation in Lead of the Whipple Meteor Bumper." Journal of Applied Physics, 31:2118-2120. 1960.
27. Pearse, R. W. B. and A. G. Gaydon. The Identification of Molecular Spectra. (Third Edition) New York: John Wiley and Sons, 1963.
28. Rautenberg, T. H. Jr. and P. D. Johnson. "Light Production in Aluminum-Oxygen Reaction." Journal of the Optical Society of America. 50:602-606, June, 1960.
29. Recht, R. F. "Catastrophic Thermoplastic Shear". Journal of Applied Mechanics. 31:189-193. 1964.
30. Richmann, J. L. Damage Assessment Technique. AFATL - TR - 67-48. Eglin Air Force Base, Florida. May, 1967.
31. Rinehart, J. S. "On Fractures Caused by Explosions and Impacts." Quarterly of the Colorado School of Mines. 55: October, 1960.
32. Tawde, N. R. and S. A. Trivedi. "CN and AlO Bands in the Study of the Carbon Arc." The Proceedings of the Physical Society. 51:733-740. November, 1939.
33. Thompson, W. T. "An Approximate Theory of Armor Penetration." Journal of Applied Physics. 26:80. 1955.
34. White, E. L. and J. J. Ward. Ignition of Metals in Oxygen. DMIC Report 224. Columbus, Ohio: Defense Metals Information Center, February, 1960.
35. White, W. C. "Suppression of AlO in the Wake of Ultraspeed Pellets." Journal of Astrophysics. 121 (1) 1955, 271-276.
36. White, W. C. "Ablation from Aluminum Ultraspeed Pellets." Journal of Astrophysics. 122 (3) 1955, 559-564.
37. Zel'dovich, Ya. B. and Ya. P. Raizer. Physics of Shock Waves and High Temperature Hydrodynamic Phenomena. Edited by T. H. Hayes and A. F. Probstein (First English Edition). New York: Academic Press, 1966.

Appendix A

Description of Equipment

The Air Force Flight Dynamics Laboratory (FDG) Ballistic Impact Test Facility Range 1 was used in this investigation. The facility located in Building 45, Area B, Wright-Patterson Air Force Base, Ohio is a 240' tunnel with remote stations for recording instrumentation and gun firing. The overall facility is described in Figure 14.



1. Flight Dynamics Laboratory Fragment Simulator

The Flight Dynamics Laboratory Fragment Simulator is a

50 caliber smooth bore gun. The chamber accepts a standard military 50 caliber casing which is percussion fired by an electrically operated solenoid. The powder charge used for all firings in this series of tests was 240 grains of Dupont 30⁰¹. The intermediate baffle plates were positioned to prevent large volumes of gas following down range and to serve as safety shields for instrumentation.

2. Instrumentation

Velocity Measurements. The velocity was measured over a two foot distance five feet prior to the target plate. The continuous line printed circuit paper screens were located two feet apart, and when the projectile passed through them a pulse was transmitted to the Beckman Universal Timer, model 7360A. The read out was in microseconds, and the velocity to the nearest ten feet per second was determined from a table prepared by the author. The maximum error introduced by this computation was $\pm 0.25\%$, which is very small when compared with the variations in velocity due to launching differences.

Streak Camera System (Figure 15). This system consisted of a reel-type Wollensack 16mm Fastax Camera and a reflective tape grid system for a background. A Hewlett-Packard time mark generator was used to mark the film at 1 millisecond intervals so that film speed could be calculated.

Because the film and event were moving on mutually perpendicular axes the time versus distance relation of down range events could be determined.

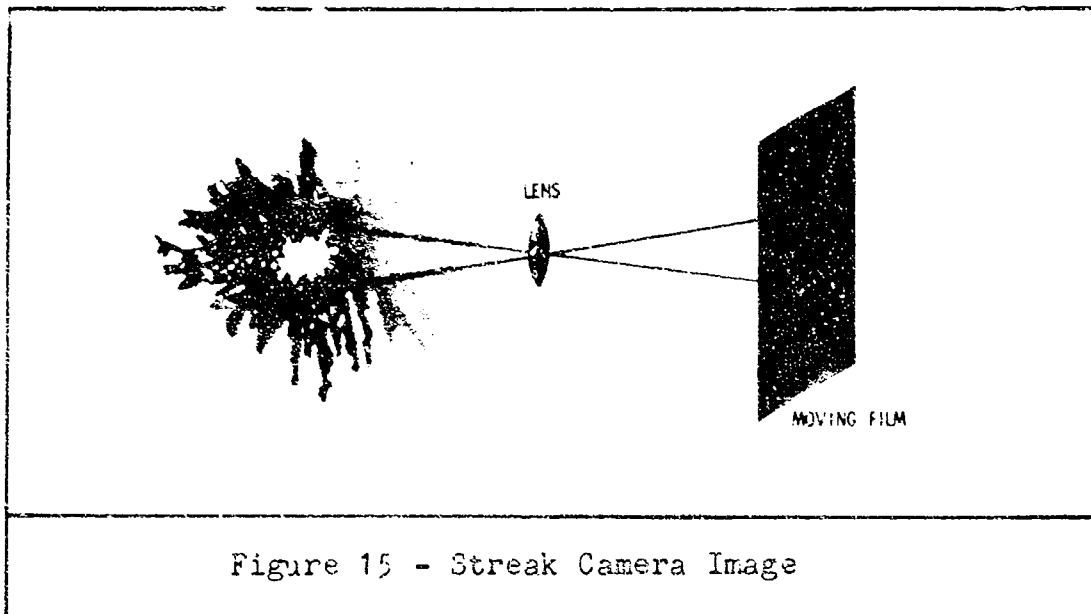
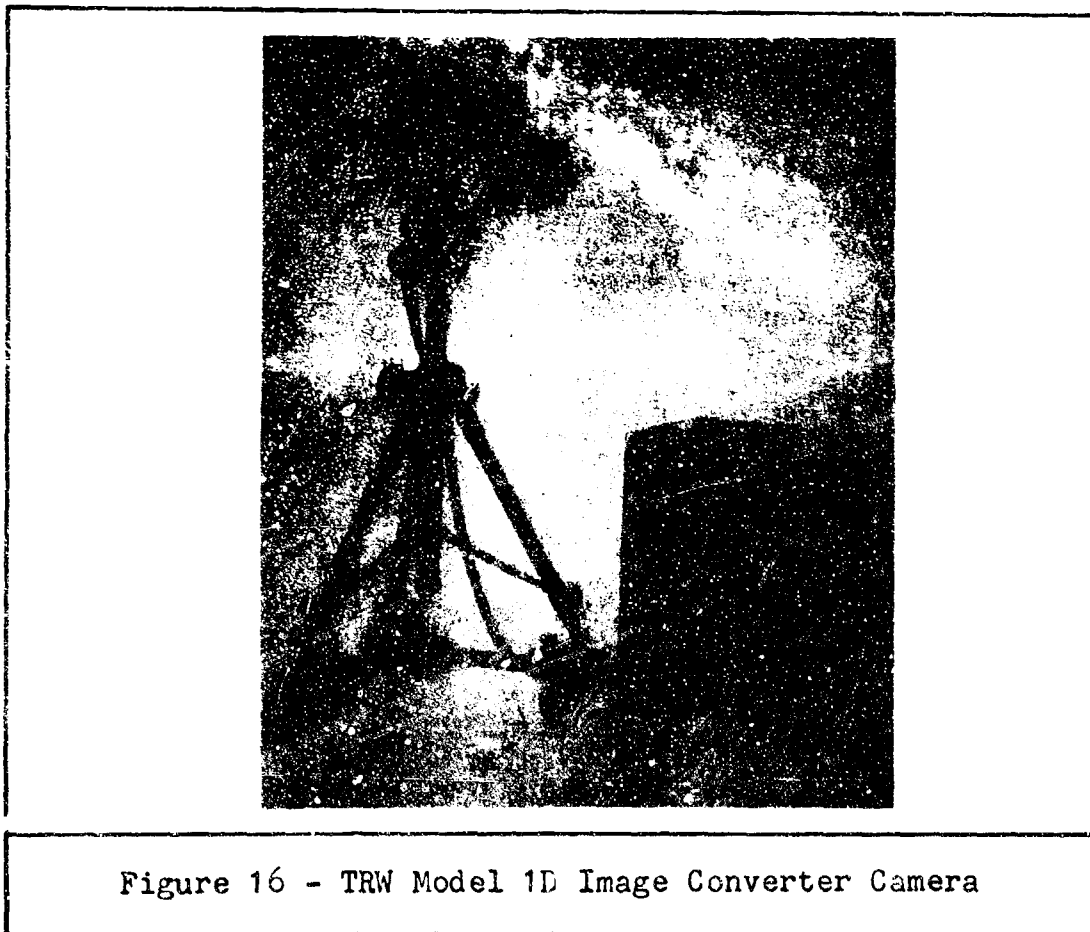


Figure 15 - Streak Camera Image

TRW Model 1D Image Converter Camera (Figure 16). The Image Converter Camera provided a capability to record time-resolved spatial and intensity data from the luminous event. The Model 1D system consists of an Objective Lens, Image Converter Tube, Relay Lens, Film Holder, Plug-in Unit, and a Power Supply Control Console. The photocathode transforms the photon image to an electron image, permitting shuttering and amplification to be accomplished electronically. The electron image is focused to cross between the deflection plates for distortion-free image deflection and is imaged on the photoanode where it is converted into a higher intensity photon image. The photon image is relayed to the film by a specially developed double-coated lens system. Triggering is accomplished by

light from the event itself. The Model 2A Trigger Delay Generator (with fiber optics input) senses the luminous event and triggers the camera. The delay programmed into the Trigger Delay Generator allows the recording of random events at preselected times.



General Electric Closed Circuit Television. The General Electric Closed Circuit Television system was used as a range safety device. The remote camera head was located so that it could scan the gun test area. The range safety officer was able to clear the range area and monitor the event from his remote location in the control room.

Spectrograph (Figure 17).

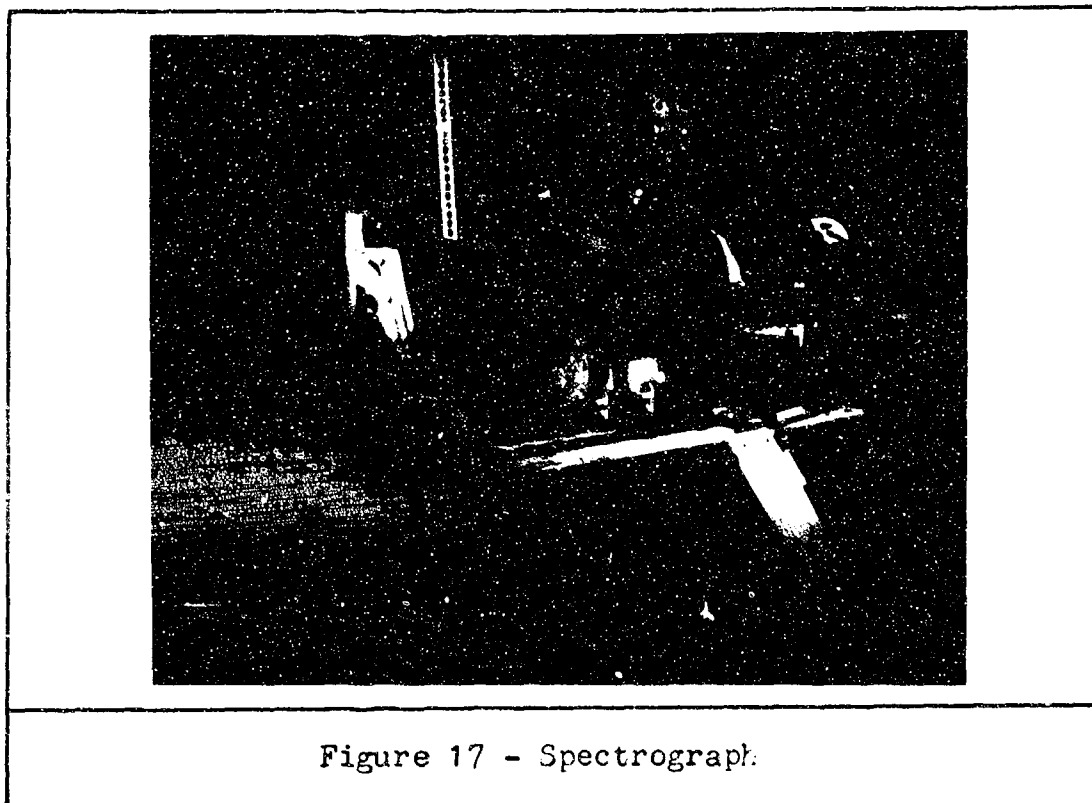


Figure 17 - Spectrograph.

The system consisted of a Barnes Engineering Company Model 18-134 Cine Spectrograph, a 5" diameter $f/4$ lens, and an adjustable slit opening. The Model 18-134 is a high-resolution instrument for photographing point source illumination. To overcome the limitation imposed by this restriction, it was necessary to align a collimating lens and a slit aperture. (Figure 6).

The spectrograph employs a Maksutov optical system (Figure 18) to achieve aberration-free images on a flat field. The optical system is corrected throughout the range from 0.2 microns to 2.6 microns. Invar bars maintain the correct spacing of the optical elements so that the instrument remains in focus even during temperature

fluctuations.

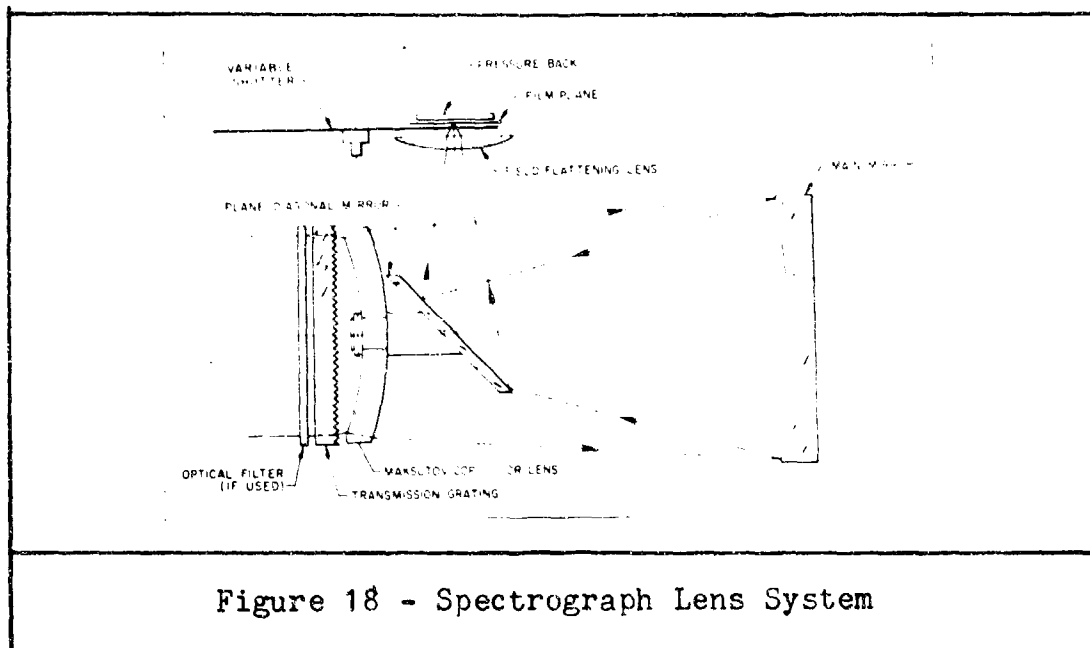


Figure 18 - Spectrograph Lens System

The optical system has an aperture ratio of $f/2.4$, which is reduced by the central obscuration to an effective ratio $f/2.7$; a very high speed for this type of objective. All optical elements other than the field flattening lens, which is recessed into the camera aperture plate, are contained in a cast magnesium optical barrel. The lens is attached to the camera with a specially designed lens mount which maintains accurate centering and positioning. The grating constants for this instrument are as follows:

Spectral Region	0.30 to 0.55 microns
Ruling	400 grooves/mm
Blazed Wave Length	0.40 microns
Dispersion	85A/mm
Spectral Resolution	1.5A
Grating Material	Epoxy on Quartz Substrate

Pyrometer. A Pyro Photomatic optical pyrometer was used in the transient mode to obtain an optical system coupled to a photomultiplier. The anode of the photomultiplier was connected to the input channels of a Techtronics Model dual trace oscilloscope. The two oscilloscope sweeps were set to different time bases to provide selective coverage of the event. The scope sweep was triggered by the TRW trigger system. The pyrometer had an effective wave length of 6500 A, and the photomultiplier was an RCA 7265, 14 stage S-20 broad band response. The limited field of view (.75 inches diameter at 48" focal distance) was found to be a severe limitation due to variations in the impact point. The event frequently was outside the direct viewing area.

Still Camera. A 4x5 "Graphex" was used to take an overall picture of the flash. Initially it was modified to an f number of about 128 in an effort to see directly into the front face flash. Kottenstette and Wittrock had reported that there was a suitable light emission called "first light" to be used as a strobe with a polaroid camera that was stopped down to a very small aperture (Ref 22:1). The attempts to determine projectile attitude and shape by this method were not successful.

Appendix B

Film Calibration

To determine relative intensities from the spectrographic plates, it was necessary that a calibration be performed to yield the relationship between relative intensity, wave length, and photographic density (amount of silver deposited on the plate). Calibration spectra were obtained from a General Electric NBS source lamp with a known intensity input, and a Penray quartz lamp was used to locate desired wave lengths on the film plates. A series of neutral density filters (Kodak .3, .5, 1.0, 2.0) were used to reduce the level of the incident light by known amounts.

The plates were developed in fresh Kodak D-76 solution at a temperature of 68^oF. with constant agitation for 10 minutes. After development the plates were washed for 30 seconds with constant agitation and then placed in fixing solution for 10 minutes with constant agitation for the first two minutes. The final washing was for a minimum of 30 minutes.

The long development time for the plates resulted in some decrease in the intensity range which could be obtained with the plates, but the time was found necessary to bring out the finer features of the band structure.

GAW/MC/68-1

The percent relative transmission of the film plates was determined with a Jarrell-Ash recording densitometer. The common logarithm of the reciprocal of the transmission for each desired wave length was plotted against incident exposure $E = (I \times t)$ (Ref 15:145). It was decided that a suitable characteristic curve could be found for each band system rather than the individual bands within the system. These curves were then plotted and, by assuming reciprocity ($I_1 t_1 = I_2 t_2$); used to relate subsequent densitometer traces to relative intensity.

Appendix CTemperature Computation Program

The following "FOR-TO-GO" program was used to determine the values of $\log \left[\sum \frac{I_{em}^{v'v''}}{\nu_{v'v''}^4} \right]$ to be plotted against the term values for the various energy levels of the excited state. The information required for the program are wave number and intensity readings. The wave numbers are to be input first in a row-wise array followed by the intensity values similarly arranged. The output information will be an adjusted intensity table with the 0-0 element as the 100 base; a Transition Probability Table; the individual element values of $\frac{I_{em}^{v'v''}}{\nu_{v'v''}^4}$; and finally the computed $\log \left[\sum \frac{I_{em}^{v'v''}}{\nu_{v'v''}^4} \right]$ for the term values.

C C RELATIVE INTENSITY PROGRAM

```

DIMENSION WL(8,8),TINT(8,9),SUM(8,9),VAXIS(8),RTRP(8)
100 READ,((WL(I,J),J=1,8),I=1,8)
    READ,((TINT(I,J),J=1,8),I=1,8)
    PUNCH 203
    PUNCH 204
    PUNCH 205
    DIV=TINT(1,1)
    DO 5 I=1,7
    DO 4 J=1,7
4    TINT(I,J)=(TINT(I,J)/DIV)*100.
    IKL=I-1
    PUNCH 201,IKL,(TINT(I,K),K=1,7)
5    CONTINUE
    PUNCH 202
    PUNCH 204
    PUNCH 205
    DO 6 I=1,7
    SUM(I,1)=0.
    DO 3 J=2,8
    TINT(I,J-1)=(TINT(I,J-1)/1000.)*(WL(I,J-1)/1000.)*4
3    SUM(I,J)=SUM(I,J-1)+TINT(I,J-1)
    F(SUM(1,8))45,44,45
44    DO 22 K=1,7
22    RTRP(K)=0.
    ICT=I-1
    PUNCH 201,ICT,(RTRP(K),K=1,7)
    GO TO 6
5    DO 2 K=1,7
2    RTRP(K)=TINT(I,K)/SUM(I,8)
    ICT=I-1
    PUNCH 201,ICT,(RTRP(K),K=1,7)
    VAXIS(I)=LOG(SUM(I,8))
6    CONTINUE
    PUNCH 206
    PUNCH 200,((TINT(II,KK),KK=1,7),II=1,7)
    PUNCH 205
    PUNCH 200.(VAXIS(I),I=1,7)
    GO TO 100
200  FORMAT(9X,7F7.2)
201  FORMAT(7X,I1,F8.2,6F7.2)
202  FORMAT(//,24X,22HTRANSITION PROBABILITY,/,1X)
203  FORMAT(//,26X,18HRELATIVE INTENSITY,/,1X)
204  FORMAT(13X,1H0,6X,1H1,6X,1H2,6X,1H3,6X,1H4,6X,1H5,6X,1H6)
205  FORMAT(1X)
206  FORMAT(///,1X)
    STOP
    END

```

Relative Intensity

V'	V'' 0	1	2	3	4	5	6
0	100.00	45.00	36.80	0.00	0.00	0.00	0.00
1	40.50	21.60	35.80	23.00	0.00	0.00	0.00
2	22.50	26.80	20.10	27.90	15.60	0.00	0.00
3	17.90	12.20	17.90	0.00	12.80	10.10	0.00
4	0.00	7.22	9.14	15.00	0.00	9.93	6.50
5	0.00	0.00	7.29	8.23	4.27	0.00	8.48
6	0.00	0.00	0.00	3.66	3.09	5.71	0.00

Transition Probability

V'	V'' 0	1	2	3	4	5	6
0	0.48	0.26	0.26	0.00	0.00	0.00	0.00
1	0.24	0.21	0.31	0.24	0.00	0.00	0.00
2	0.14	0.19	0.18	0.29	0.20	0.00	0.00
3	0.00	0.16	0.28	0.00	0.29	0.27	0.00
4	0.00	0.00	0.16	0.31	0.00	0.30	0.23
5	0.00	0.00	0.00	0.62	0.38	0.00	0.00
6	0.00	0.00	0.00	0.50	0.50	0.00	0.00

$$\left[\frac{I_{em}^{v'v''}}{z^{4v''}} \right]$$

V'	V'' 0	1	2	3	4	5	6
0	54.97	29.95	29.85	0.00	0.00	0.00	0.00
1	18.91	16.60	24.26	18.96	0.00	0.00	0.00
2	8.99	12.77	11.48	19.22	13.04	0.00	0.00
3	0.00	4.98	8.69	0.00	8.95	8.56	0.00
4	0.00	0.00	3.80	7.42	0.00	7.04	5.57
5	0.00	0.00	0.00	3.49	2.15	0.00	0.00
6	0.00	0.00	0.00	1.34	1.33	0.00	0.00

A10 System Excited By Carbon Arc (Ref 32;734)

Table VI

Relative Intensity

V'	V''	0	1	2	3	4	5	6
0	0	100.00	35.00	35.00	0.00	0.00	0.00	0.00
1	0	45.00	35.00	25.00	10.00	0.00	0.00	0.00
2	0	15.00	25.00	15.00	20.00	5.00	0.00	0.00
3	0	0.00	10.00	15.00	0.00	15.00	5.00	0.00
4	0	0.00	0.00	10.00	15.00	0.00	10.00	0.00
5	0	0.00	0.00	0.00	10.00	10.00	0.00	5.00
6	0	0.00	0.00	0.00	0.00	15.00	0.00	0.00

Transition Probability

V'	V''	0	1	2	3	4	5	6
0	0	0.32	0.22	0.27	0.00	0.00	0.00	0.00
1	0	0.32	0.30	0.26	0.13	0.00	0.00	0.00
2	0	0.13	0.27	0.19	0.31	0.09	0.00	0.00
3	0	0.00	0.16	0.28	0.00	0.40	0.16	0.00
4	0	0.00	0.00	0.22	0.40	0.00	0.38	0.00
5	0	0.00	0.00	0.00	0.46	0.54	0.00	0.00
6	0	0.00	0.00	0.00	0.00	1.00	0.00	0.00

$$\left[\frac{I_{em}^{v'v''}}{\nu^{v'v''}} \right]$$

V'	V''	0	1	2	3	4	5	6
0	0	54.97	23.30	28.39	0.00	0.00	0.00	0.00
1	0	21.01	19.62	16.94	8.24	0.00	0.00	0.00
2	0	5.99	11.91	8.57	13.78	4.18	0.00	0.00
3	0	0.00	4.08	7.29	0.00	10.49	4.24	0.00
4	0	0.00	0.00	4.16	7.42	0.00	7.09	0.00
5	0	0.00	0.00	0.00	4.24	5.03	0.00	0.00
6	0	0.00	0.00	0.00	0.00	6.47	0.00	0.00

ALO System Excited By Aluminum Projectile

Table VII

Vita

John Billy Abernathy was born on 4 February 1936 in Cleveland, Mississippi. He attended the United States Military Academy and graduated in 1958 with a Bachelor of Science degree. After being commissioned in the Regular Air Force, he completed pilot training in 1959. He has served as a Tactical Fighter Pilot in England, Korea, Japan, Okinawa, and Southeast Asia as well as the United States. He entered the Air Force Institute of Technology in 1966.

Permanent address: 466 West Taylor Run Parkway
Alexandria, Virginia
22314

This thesis was typed by Nancy Abernathy

Unclassified

Security Classification

DOCUMENT CONTROL DATA - R & D

(Security classification of title, body of abstract and indexing annotation must be entered when the overall report is classified)

1. ORIGINATING ACTIVITY (Corporate author) Air Force Institute of Technology (AFIT-SE) Wright-Patterson AFB, Ohio 45433	2a. REPORT SECURITY CLASSIFICATION Unclassified 2b. GROUP
---	---

3. REPORT TITLE

Ballistic Impact Flash

4. DESCRIPTIVE NOTES (Type of report and inclusive dates)
AFIT Thesis

5. AUTHOR(S) (First name, middle initial, last name)

John B. Abernathy

6. REPORT DATE May 1968	7a. TOTAL NO. OF PAGES	7b. NO. OF REFS 37
----------------------------	------------------------	-----------------------

8a. CONTRACT OR GRANT NO. n/a	9a. ORIGINATOR'S REPORT NUMBER(S) AFIT Thesis GAW/MC/68-1
b. PROJECT NO. n/a	
c.	9b. OTHER REPORT NO(S) (Any other numbers that may be assigned this report)
d.	n/a

10. DISTRIBUTION STATEMENT

This document has been approved for public release and sale; its distribution is unlimited.

11. SUPPLEMENTARY NOTES	12. SPONSORING MILITARY AGENCY Air Force Flight Dynamics Laboratory Wright-Patterson AFB, Ohio 45433
-------------------------	--

13. ABSTRACT

The down range flash from the perforation of thin aluminum plates by steel and aluminum fragment simulators, one half inch diameter cylinders with hemispherical heads, was investigated to determine time, size, and temperature. By comparing the relative intensities of vibrational band structure in the ALO green system an effective vibrational temperature for the flash was determined to be between 3400°K and 4100°K. The overall dimensions of the flash were found to be approximately 14 inches in the axial direction and five inches in the transverse direction. The time duration was found to be between three and five milliseconds.

~~Unclassified~~

Security Classification

KEY WORDS	LINK A		LINK B		LINK C	
	ROLE	WT	ROLE	WT	ROLE	WT
Impact Flash Ballistic Impact						

Security Classification